Study on the dislocation sub-structures of Al–Mg–Si alloys fatigued under non-proportional loadings

Xiang-qun Ding · Guo-qiu He · Cheng-shu Chen

Abstract In this article, the fatigue dislocation sub-structures of Al–Mg–Si alloys were studied under the same equivalent stress amplitude of 93 MPa with multi-axial non-proportional loading paths, which were circle, ellipse, rectangle, and square loading paths. After fatigue test, the fatigue dislocation sub-structures of the failure specimens were also observed under different equivalent stress amplitudes, which were 47, 70, 90, 140, and 163 MPa with the transmission electron microscopy method. The results indicate that fatigue lives of the alloy are different under different loading paths with the same equivalent stress amplitude, and the fatigue life decreases with the increase in equivalent stress amplitude from 47 to 163 MPa. Cyclic additional hardening is found above medium effective stress amplitude of 93 MPa. The dislocation sub-structures strongly depend on equivalent stress amplitudes and loading paths. The dislocation sub-structures of parallel slip band, slight small dislocation cell (or labyrinth), and remarkable labyrinth feature are found under the equivalent stress amplitudes of 47, 93, and 140 MPa, respectively. The movability of the dislocation and the stress concentration degree are closely related to fatigue life and cyclic hardening of the alloy.

X. Ding (✉)
School of Material Science and Engineering, Shenyang Jianzhu University, Shenyang 110168, China
e-mail: Xiangqunding@126.com

G. He · C. Chen
School of Material Science and Engineering, Tongji University, Shanghai 200092, China

Introduction

In recent years, there has been an increasing trend in the automotive and motor-trolley industry to use Al–Mg–Si alloys [1–3]. However, to successfully use such alloys in components for long life applications requires understanding of their fatigue behaviors necessarily, especially the failure mechanism of Al–Mg–Si alloys fatigued under complex loads.

The research of fatigue under multi-axial non-proportional loadings has drawn much attention of many researchers such as Doong, Kueppers, Nishino, Wang De-gun, etc. [4–8]. The fatigue mechanism and the relationship between the dislocation sub-structures and the fatigue properties of failure materials have been studied [9, 10]. For example, He [11] observed the dislocation sub-structure of 316L steel fatigued under multi-axial non-proportional loadings, and it was found that the difference of dislocation sub-structure of the failure material is notable under different equivalent strain amplitudes. To some extent, the fatigue principle is reflected by the dislocation sub-structures. Zhu et al. [12] studied the multi-axial low cycle fatigue behavior of cast aluminum alloys ZL101 under proportional and non-proportional loadings, and found that the aluminum alloy shows cyclic hardening both under multi-axial proportional and non-proportional loadings, whereas the cyclic additional hardening with low level was shown under non-proportional loading. Doong et al. [13] studied the dislocation structure of aluminum, copper, and stainless-steel fatigued under proportional and non-proportional loadings, the results indicated that the dislocation cells were found for materials fatigued under proportional loadings, and the dislocation cells and dislocation labyrinths were found for material fatigued under non-proportional loadings. Nishino et al. [14] and

Kida et al. [15] observed the dislocation structure of stainless steel fatigued under proportional and non-proportional loadings, and found that the dislocation structure related to the non-proportional loading paths. Xiao Lin and Juli [16] studied the dislocation structure of Zr-4 alloy fatigued under multiaxial non-proportional loadings, and the different dislocation structures were found under different equivalent strain amplitudes. Shang et al. [17] studied the cyclic stress–strain relation under multi-axial proportional and non-proportional loading and derived a multi-axial cyclic constitutive relation under non-proportional loadings.

On the other hand, most of the studies about the multi-axial fatigue under non-proportional loadings were focused on steels or the macro-mechanic properties of fatigued materials. Few studies on the dislocation sub-structures of aluminum alloy fatigued under multi-axial loadings or different loading paths have been reported [8, 18–25]. Particularly, few researches have combined the fatigue behavior with dislocation sub-structure to analyze the fatigue mechanism of Al–Mg–Si alloys under multi-axial non-proportional loadings [13, 26], although the research on the dislocation sub-structure of fatigued aluminum alloy is important for its successful use in components. It is very useful to study the dislocation sub-structure of material fatigued under different equivalent stress (or strain) amplitudes.

In this article, the fatigue properties of Al–Mg–Si alloys fatigued under multi-axial loadings were tested, and the dislocation sub-structures of fatigued alloy under different equivalent stress amplitudes or different loading paths were observed. The fatigue micro-mechanism of Al–Mg–Si alloys under multi-axial loadings was also discussed, and an approximated model for aluminum alloy fatigued under multi-axial loadings was given.

Materials and methods

Material and specimen

The chemical components and mechanical properties of a commercial wrought aluminum alloy used for fatigue test are listed in Tables 1 and 2, respectively. After heat treating of T-6, the alloy was machined to a type of smooth tubular specimen for the multi-axial fatigue test (see Fig. 1).

Table 2 Mechanical properties of Al–Mg–Si alloys used

Item	Yield stress σ_s (MPa)	Ultimate stress σ_b (MPa)	Elongation δ (%)	Young's modulus E (GPa)	Shear modulus G (GPa)
Value	165	235	12	70	25.2
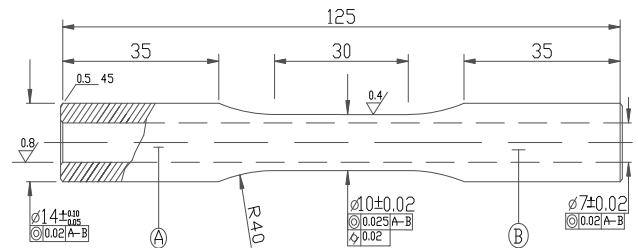
Fig. 1 Specimen with cross section for fatigue test (unit: mm)

Test procedure

Stress-controlled tension–torsion loadings tests were carried out on a servo-hydraulic MTS Model 809 axial-torsion testing system. The experiments were conducted at a room temperature of 20 °C. A low frequency of 0.5 Hz was employed when the tests were started and the frequency was increased up to 15 Hz after several tens of cycles. The stress ratio was equal to ±1 for both of axial and torsional loadings. Under the same circle loading path different equivalent stress amplitudes were chosen, which were 47, 70, 90, 140, and 163 MPa. Under the same equivalent stress amplitude of 93 MPa, different loading paths were chosen, which were circle, ellipse, rectangle, and square, and the proportional loading path was also included to make a comparison (see Table 3).
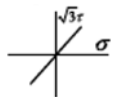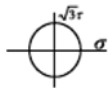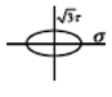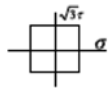
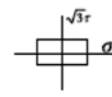### Micro-structure test

For the fatigue failure specimen, a slim piece of about 1 mm thickness was cut beneath the fracture surface. Then these slim pieces were decreased to about 50 μm thickness foils using carborundum paper. And then the foil samples were continued decreased to about 20 nm thickness with a wedge hole in them by twin-jet electro-polishing with an electrolyte consisting of 8% perchloric acid and 92% alcohol. These thin films were prepared for transmission electron microscopy (TEM) test. TEM observations were carried out by using a Hitachi H-800 transmission electron

Table 1 Chemical composition (mass%) of Al–Mg–Si alloys used

Element	Fe	Si	Cu	Mg	Mn	Zn	Cr	Ti	Al
Percent	0.1869	0.4463	0.0275	0.707	0.0288	0.0098	0.0126	0.0196	Bal.

Table 3 The illustration of different loading paths for multi-axial fatigue test

| Loading path	Proportional	Circle	Ellipse	Square	Rectangle
	$\sqrt{3}\tau$ σ	$\sqrt{3}\tau$ σ	$\sqrt{3}\tau$ σ	$\sqrt{3}\tau$ σ	$\sqrt{3}\tau$ σ
Ratio of ($\sqrt{3}\tau:\sigma$)	1:1	1:1	1:2	1:1	1:2
Control waveform	Sinusoidal	Sinusoidal	Sinusoidal	Trapezoidal	Trapezoidal
Phase difference (θ)	0°	90°	90°	90°	90°

microscope operated at 200 kV, equipped with a conventional double tilting stage.

Results and discussion

Fatigue test results

Table 4 shows the fatigue results of the Al–Mg–Si alloys under the same circle loading path with different equivalent stress amplitudes. As can be seen, the fatigue life of the alloy decreases with the increase in the equivalent stress amplitude from 47 to 163 MPa. From the energy viewpoint of fatigue damage, the damage is heavier under a bigger loading and results in a lower fatigue life. The fatigue life of the alloy exceeds 5×10^4 cycles below the equivalent stress amplitude of 93 MPa (just a little higher than half of the alloy's yield stress), and the fatigue life of the alloy is lower than 5×10^4 cycles above the equivalent stress amplitude of 117 MPa. So, the equivalent stress amplitude 93 MPa may be a critical value separating the high cycle from low cycle fatigue of Al–Mg–Si alloys under multiaxial non-proportional loadings.

Figure 2 shows the effective strain amplitude variation during the cyclic loading under the circle loading path with the equivalent stress amplitude ranged from 47 to 163 MPa. Cyclic additional hardening can be found slightly above the effective stress amplitude 93 MPa, and it becomes more and more remarkable with the increase in equivalent stress amplitude. The alloy exhibits cyclic additional hardening during the initial 100 cycles, and then the equivalent strain amplitude tends to stable gradually. The cyclic additional hardening could not be found below the equivalent stress amplitude of 70 MPa (see Fig. 2). The equivalent stress amplitude of 93 MPa is a critical value separating the cyclic additional hardening, and so it was
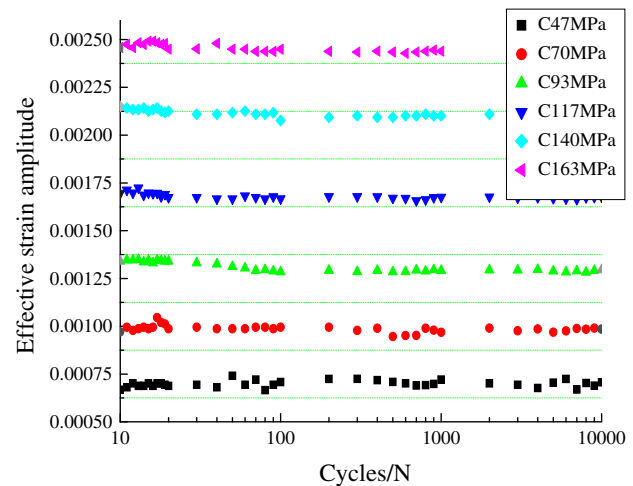
Fig. 2 The equivalent strain amplitude versus fatigue life under circle loading path with different equivalent stress amplitudes

chosen as the equivalent stress amplitude for fatigue test under different loading paths.

Table 5 lists the fatigue results of the alloy under different loading paths with the same equivalent stress amplitude 93 MPa. As shown in the table, the fatigue life is arrayed by the sequence as follows: proportional > ellipse > rectangle > square > circle according to the loading path. The fatigue life of every tested alloy exceeds 5×10^4 cycles. From the energy viewpoint of fatigue damage, the circle loading brings the maximum damage to the alloy and results in the lowest fatigue life. The proportional loading path leads to the smallest damage and results in the longest fatigue life. The other loading paths cause smaller damages than the circle path and therefore results in relatively longer fatigue lives.
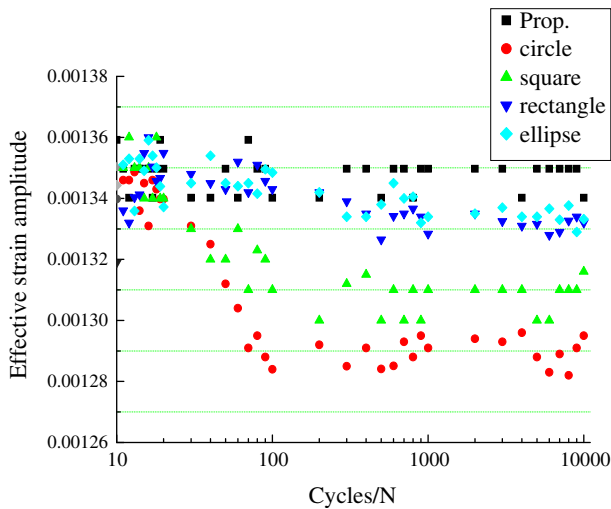
Figure 3 shows the equivalent strain amplitude variation during the cyclic loading under the same effective stress amplitude with the circle, ellipse, rectangle, and square

Table 4 Fatigue life of the alloy under the same circle loading path with different equivalent stress amplitudes

Equivalent stress amplitude (MPa)	47	70	93	117	140	163
Fatigue life (cycles)	$>1.0 \times 10^7$	2.2×10^6	6.0×10^4	1.7×10^4	4.3×10^3	1.7×10^3

Table 5 Fatigue life under different loading paths with the same equivalent stress amplitude 93 MPa

Loading path	Proportional	Ellipse	Rectangle	Square	Circle
Fatigue life (cycles)	1.6×10^6	1.3×10^5	8.1×10^4	6.8×10^4	5.9×10^4

Fig. 3 The effective strain amplitude versus fatigue life of the alloy under different loading paths with the same equivalent stress amplitude of 93 MPa

loading paths, respectively. The alloy expresses the cyclic additional hardening under different loading paths except for the proportional loading path. The effective strain amplitude is arrayed by the same sequence as that of the fatigue life as follows: proportional > ellipse > rectangle > square > circle, and the effective strain amplitude of circle loading path is lowest in the fatigue-stabilized stage.

Dislocation sub-structure

Dislocation sub-structure under different equivalent stress amplitudes

Figure 4 shows TEM images of the alloy fatigued under the same loading path with different equivalent stress amplitudes. All of the images were shot from the crystal axial line of aluminum.

Under the equivalent stress amplitude of 47 MPa, the dislocation bands array in one direction, the directivity of the dislocations in another direction is not clear. The dislocation density is high (see Fig. 4a). In the higher magnification image (Fig. 4b), long and bend dislocation lines tangle each other, especially around the second phase particles.

Under the equivalent stress amplitude of 93 MPa, the dislocation structure slightly likes a labyrinth, the dislocation density is extremely high (see Fig. 4c). Many dislocation fragments and ring-like dislocations are found in the higher magnification image (Fig. 4d).

The dislocation density is extremely high with obvious labyrinth structure under equivalent stress amplitude of 140 MPa (Fig. 4e). In the higher magnification image (Fig. 4f), a large number of short dislocation lines, small pieces, and ring-like dislocations are found.

Figure 4 shows that the dislocation sub-structure with a labyrinth feature is more and more obvious with the increase in equivalent stress amplitude. The dislocation density, quantity of short dislocation lines, dislocation fragments, and ring-like dislocations all increase with the increase in equivalent stress amplitude.

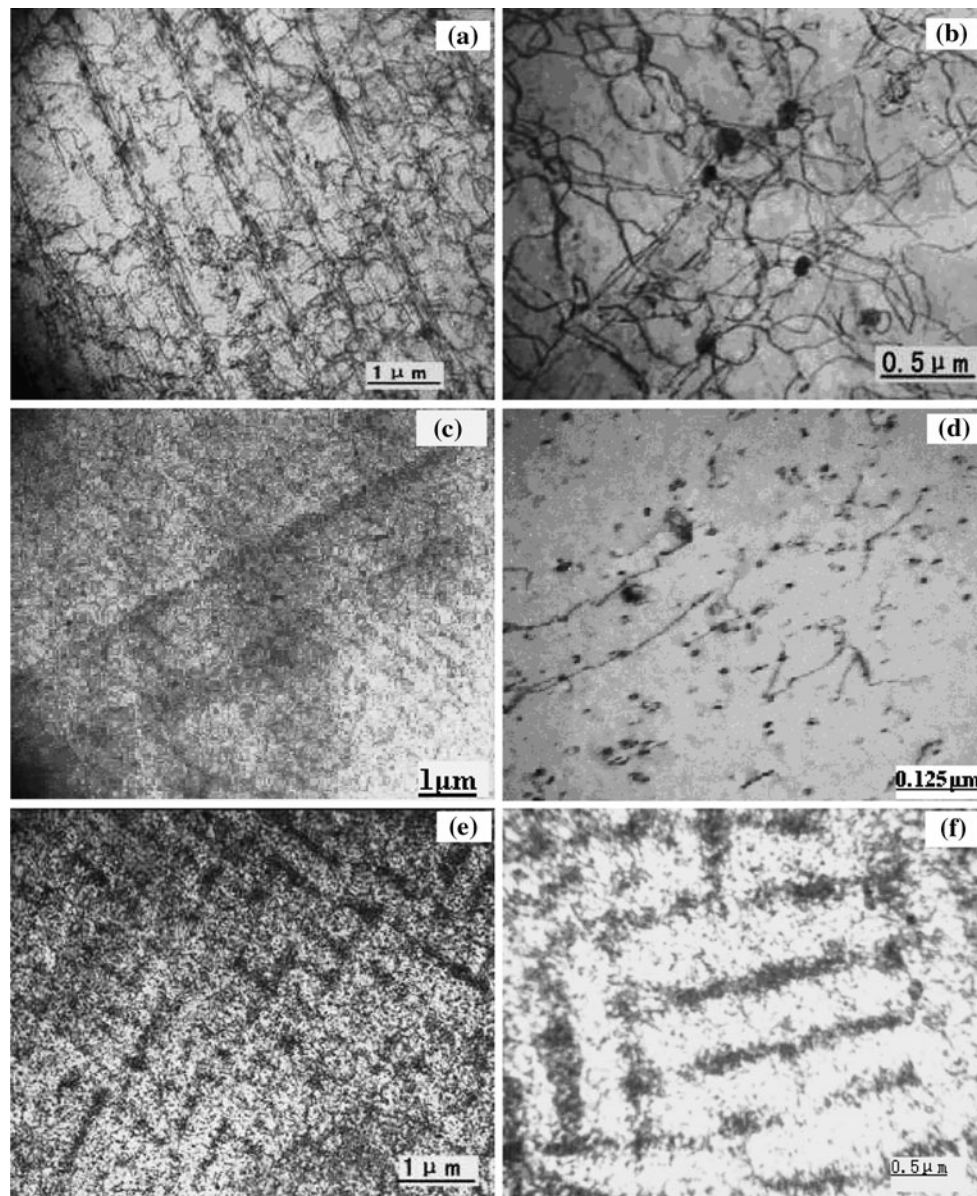*Dislocation sub-structures under different loading paths*

Figure 5 shows the TEM images of the alloy fatigued under different loading paths with the same equivalent stress amplitude except under the circle loading path, which is shown in Fig. 4 and described above.

The dislocation bands array in two directions under ellipse loading path, the crossed dislocation bands form many small parallelogram grids, in which there are many congested dislocations (see Fig. 5a). Long dislocation lines restrict each other in two directions, and the dislocations crow around the second phase particle. It can be found that the movability of dislocation decreases compared with that under circle loading path in the higher magnification image (Fig. 5b).

Similar to those under ellipse path, the dislocation bands array in two directions under rectangle loading path, the crossed dislocation bands form many small parallelogram grids, in which there are many congested dislocations (see Fig. 5c). The dislocation lines arrayed in different directions tangle each other, and the dislocation also crow around the second phase particle. The movability of dislocation is lower compared with that under ellipse path in the higher magnification image (Fig. 5d). The directivity of crossed dislocation bands is distinct for ellipse and rectangle loading paths.

Similar to those under circle loading path, the dislocation sub-structure with slight labyrinth feature is found under square loading path. But the labyrinth feature is unclear, and the dislocation density is also lower comparing with that under circle loading path (see Fig. 5e). Many

Fig. 4 The dislocation sub-structures of the alloy fatigued under circle loading path with different equivalent stress amplitudes: **a**, **b** 47 MPa, **c**, **d** 93 MPa, **e**, **f** 140 MPa

dislocation fragments and ring-like dislocations are also found in the higher magnification image (Fig. 5f), but the quantity of dislocation fragments and ring-like dislocations seems less than that under circle loading path.

Figure 5 shows that the dislocation density under different loading paths changes from low to high by the following sequence: ellipse < rectangle < square < circle. On the contrary, the dislocation movability changes by the sequence as follows: ellipse > rectangle > square > circle.

Under circle loading path with the equivalent stress amplitude of 93 MPa, the parallel dislocation lines array near the second phase particle, and the dislocations also tangle around this particle (see Fig. 6).

Micro-mechanism discussion of Al–Mg–Si alloys fatigued under multi-axial non-proportional loadings

Effect of the equivalent stress amplitude on the fatigue behavior

Under circle loading path, the dislocations move easier and faster under a high equivalent stress amplitude than under a low equivalent stress. So the dislocation density is higher, and labyrinth feature is also more and more obvious with the increase in equivalent stress amplitude. All of these result in a harder movement of dislocation under a high stress than under a low stress. This will lead to more severe
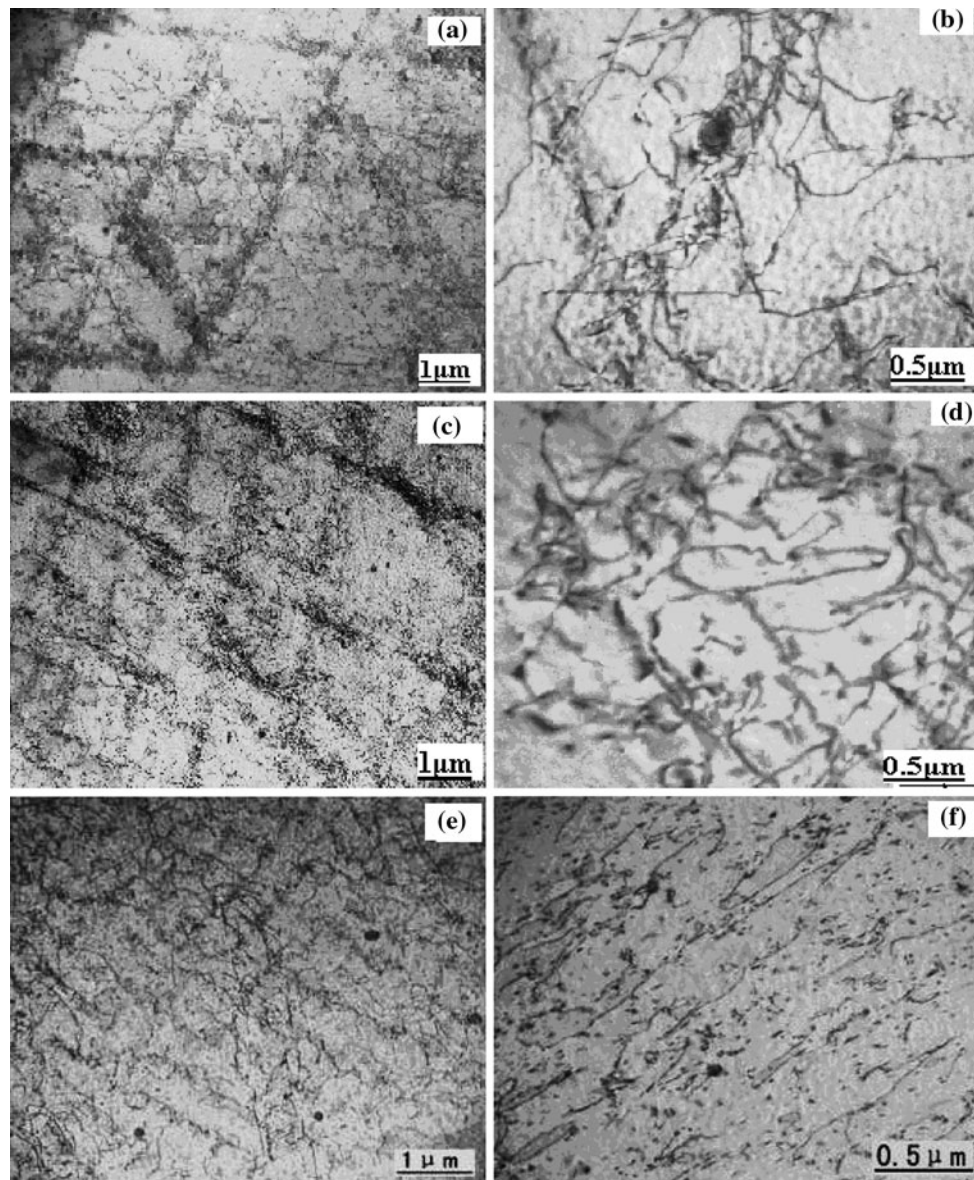
Fig. 5 The dislocation sub-structure of the alloy fatigued under different loading paths with the same equivalent stress amplitude of 93 MPa: **a**, **b** ellipse path, **c**, **d** rectangle path, **e**, **f** square path

cyclic hardening (defined as a process, in which the strain amplitude of the material deforming under constant cycle stress decreases with the increase in cycle number, until the strain amplitude stable. Some researchers believed that the cyclic hardening is because of the accumulated damage and the increase in deformation resistance of materials under constant cycle stress or strain. The cyclic hardening was also found in 316(316L) stainless steel and Al–Mg–Si alloys fatigued under multi-axial proportional loadings [27–30]). So the stress concentration under higher equivalent stress amplitude is more severe, and micro-cracks will initiate easier in this case. Naturally, the fatigue life of the alloy is short. Because of the severe dislocation reaction or the connection of bend dislocation end to end under high
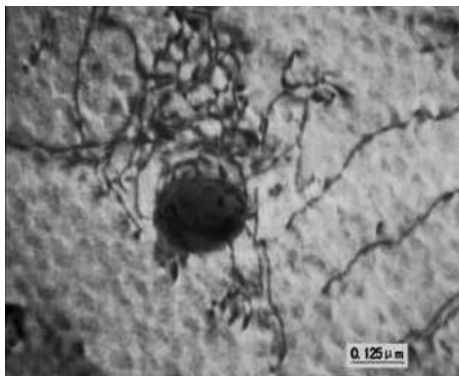
equivalent stress amplitudes, many dislocation fragments and ring-like dislocations are found by TEM.

Based on the above analysis, it is quite obvious that the equivalent stress amplitude exerts a vital effect on the fatigue life of the alloy under circle loading path. The different dislocation sub-structures can reflect the fatigue behavior of Al–Mg–Si alloys under multi-axial non-proportional loadings to a great extent.

Effect of different loading paths on the fatigue behavior

The maximum shear stress plane alternate all the time. The alloy undergoes the maximum stress during the whole process under circle loading path with the same equivalent

Fig. 6 The parallel dislocation lines array near the second phase particle under circle loading path with the equivalent stress amplitude of 93 MPa

Fig. 7 Prediction of fatigue life of Al–Mg–Si alloys under circle loading path (Eq. 1)

stress amplitude of 93 MPa. So the dislocations move easy and fast in this condition. The dislocation movement becomes very hard and difficulty. The stress concentration level and accumulative damage degree of the alloy become severe. Naturally, all of these result in a severe cyclic additional hardening and short fatigue life of Al–Mg–Si alloys under circle loading path.

On the other hand, the alloy undergoes the maximum stress acting at two points during every cycle with the same equivalent stress amplitude under ellipse loading path. The stress under ellipse loading path at other points is lower than that under circle loading path. Comparing with circle loading path, the dislocations move harder and slower under ellipse loading path. So the dislocation movement becomes easy for ellipse loading path, and the dislocation resistance decreases. The stress concentration level and accumulative damage degree of the alloy become slight. Hence, slight cyclic additional hardening and long fatigue life of Al–Mg–Si alloys under ellipse loading path are found.

For the rectangle and square loading paths, the dislocation movability as well as stress concentration degree is just between that for circle and ellipse loading paths. Naturally, the cyclic additional hardening and fatigue life under rectangle and square loading paths are between those under circle and ellipse loading paths.

The approximated model

Based on the study of fatigue properties and dislocation sub-structures of Al–Mg–Si alloys fatigued under multi-axial non-proportional loadings, as the damage parameters, the maximum shear stress and the non-proportionality reflecting the effect of loading path on fatigue property were introduced to the fatigue life prediction model (see Eq. 1) (a new measure of non-proportionality defined with
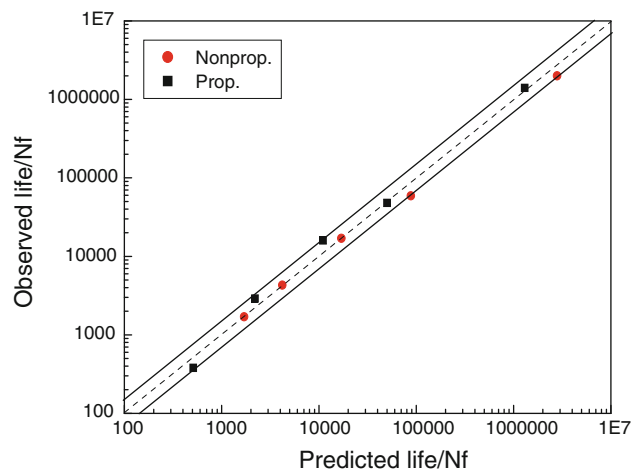
$\bar{S}^{-1}$ of statistical mean value $(\bar{S})$ between the effective saturation stress amplitude and the spacing of between movement-free dislocations under multi-axial non-proportional loading by He, the non-proportionality for circle loading path is 0.75 [29, 30]).

$$\frac{\Delta\gamma_{\max}}{2} + \frac{\Delta\varepsilon_{\max}^n}{2} = (2 + v_e)\frac{\sigma_f'}{E}(2N_f)^{b_0}$$
$$+ (1 + L_2\Phi)^{\frac{-1}{n}}(2 + v_p)\varepsilon_f'(2N_f)^{c_0} \qquad (1)$$

where $\Delta\gamma_{\max}$ and $\Delta\varepsilon_{\max}^n$ are the amplitude of maximum shear strain and maximum normal strain acting on the plane, respectively, v_e and v_p are elastic and plastic Poisson ratios, respectively, σ_f' and ε_f' are the strength factor and ductility factor of material fatigued under tensile compression loading, E is elastic modulus of tensile compression, b_0 and c_0 are intensity index and ductility index of material fatigued under tensile compression loading, L_2 is the additive strengthening factor of material fatigue under non-proportional loadings, Φ is the non-proportionality under different loading paths, N_f is the fatigue life of Al–Mg–Si alloys fatigued under multi-axial non-proportional loadings.

Equation 1 is useful to predict the fatigue life of Al–Mg–Si alloys under multi-axial proportional and non-proportional loadings with circle loading path (Fig. 7). It will be discussed carefully in other paper.

Conclusions

According to the study of fatigue behavior and dislocation sub-structure of Al–Mg–Si alloys under circle loading path with different equivalent stress amplitudes, both of the dislocation sub-structure and fatigue behavior of the alloy exhibit a close relation to the equivalent stress amplitude.

The alloy shows severer cyclic additional hardening and lower fatigue life under higher equivalent stress amplitudes than under lower equivalent stress amplitudes. The alloy is found to exhibit a labyrinth structure of dislocation under equivalent stress amplitude of 140 MPa, and the movement of dislocation becomes extremely hard in this case. Comparably, the alloy shows a dislocation band with one direction under equivalent stress amplitude of 47 MPa, and the movement of dislocation is easier than that under equivalent stress of 93 or 140 MPa.

Under different loading paths with the same equivalent stress amplitude of 93 MPa, both of the dislocation substructure and fatigue behavior of the alloy depend on the type of the loading path. Under circle loading path, the alloy shows the severest cyclic additional hardening and is found to exhibit a preliminary labyrinth structure of dislocation. The movement of dislocation is extremely hard in this condition. All of this result in shortest fatigue life of the alloy. Contrary to under circle loading path, the alloy under ellipse path exhibits a lighter cyclic hardening and longer fatigue life. The dislocation sub-structure is cross-slipping bands with different directions. The dislocation movement is easier than that under circle loading path.

References

1. Ding X, He G, Chen C et al (2005) J Tongji Univ 33(11):1504
2. Engler O, Hirsch J (2002) Mater Sci Eng 40(2):249
3. William K (2003) Automotive Eng 28(4):54
4. Doong SH, Socie DF (1991) J Eng Mater Technol 113:23
5. Kueppers M, Sonsino CM (2006) Int J Fatigue 28:540
6. Dejun WANG (2002) Chin J Mater Res 16:439
7. Xia Z, ElIyin F (1998) Int J Fatigue 20(1):51
8. McDowell GW (1997) Int J Fatigue 19(1):32
9. Lados Diana A (2004) Mater Sci Eng A385:200
10. Cailletaud G, Doquet V, Pineau A (1991) In: Kussmaul K et al (eds) Fatigue under biaxial and multiaxial loading, vol 10. ESIS, London, pp 131–149
11. He G (1995) PhD thesis, Solid Mechanics Department of Southwest Jiaotong University, Chengdu, China, pp 56–66
12. Zhu Z-y, He G-q, Ding X-q, Liu X-s, Zhang W-h (2007) Chin J Nonferrous Met 17(6):916
13. Doong SH, Socie DF, Robertson IM (1990) Eng Mater Technol 112:456
14. Nishino S, Hamada N, Sakane M et al (1986) Fatigue Fract Eng Mater Struct 9(1):65
15. Kida S, Itoh T, Sakane M et al (1997) Fatigue Fract Eng Mater Struct 20:1375
16. Lin X, Juli B (2000) J Met 36(9):919
17. Shang D, Yao W, Wang D (1999) Chin J Appl Mech 16(3):66
18. Xue Y, McDowell DL, Horstemeyer MF (2007) Eng Fract Mech 74:2810
19. Liu Y, Mahadevan S (2005) Int J Fatigue 27:790
20. Gan J, Vetrano JS, Khaleel MA (2002) J Eng Mater Technol 124(7):297
21. Desmukh MN, Pandey RK, Mukhopadhyay AK (2005) Scr Mater 52:645
22. Fujii T, Watanabe C, Nomura Y et al (2001) Mater Sci Eng A 319–321:592
23. Zettl B, Mayer H, Stanzl-Tschegg SE, Degischer HP (2001) Mater Sci Eng A292:1
24. McDowell DL, Gall K et al (2003) Eng Fract Mech 70:49
25. Banvillet A et al (2003) Int J Fatigue 25:755
26. He G et al (1997) J Southwest Jiaotong Univ 24(3):423
27. Suresh S (1998) Fatigue of materials, 2nd edn. Cambridge University Press, London
28. Wang S (1985) Fatigue of metal. Fuzhou Science and Technology Press, Fuzhou
29. He G (1995) PhD thesis, Southwest Jiaotong University, China
30. Ding X (2006) PhD thesis, Tongji University, China